ELSEVIER

Journal of Chromatography A, 883 (2000) 39–54

JOURNAL OF CHROMATOGRAPHY A

www.elsevier.com/locate/chroma

# Pore size distributions of cation-exchange adsorbents determined by inverse size-exclusion chromatography

Peter DePhillips[a,b], Abraham M. Lenhoff[c,*]

[a]*Merck Research Laboratories, Sumneytown Rd., West Point, PA 19486, USA*
[b]*Department of Chemistry and Biochemistry, University of Delaware, Newark, DE 19716 USA*
[c]*Department of Chemical Engineering, University of Delaware, Newark, DE 19716, USA*

Received 12 August 1999; received in revised form 2 March 2000; accepted 28 March 2000

**Abstract**

The pore dimensions, pore size distributions, and phase ratios were determined for a set of cation-exchange adsorbents using inverse size-exclusion chromatography (ISEC). The adsorbents examined represent a diverse set of materials from Pharmacia, TosoHaas, BioSepra, and EM Industries, which are widely used for protein purification. The ISEC was carried out using dextran standards with relative molecular masses of 180–6 105 000. This technique provided a comparative characterization of the accessible internal pore surface area, as a function of solute size, for the adsorbents tested. Adsorbent preparation strategies in which polymers are generated in situ or grafted onto base materials were found to have significant effects on pore dimensions and phase ratios. 

*Keywords:* Pore size distribution; Inverse size-exclusion chromatography; Cation-exchange adsorbents; Stationary phases, LC; Ion exchangers

## 1. Introduction

Solute retention in liquid and gas chromatography is characterized by the fundamental retention equation:

$$k' = \frac{t_R - t_0}{t_0} \quad (1)$$

in which the retention factor, $k'$, is expressed in terms of experimentally obtained parameters; $t_R$ is the retention time of the solute of interest and $t_0$ is the time for an unretained solute to pass through the column. A mechanistic characterization of chromatographic retention, specific to linear adsorption, is provided by the relationship:

$$k' = K_{eq}\phi \quad (2)$$

in which solute retention is expressed as the product of two contributions. The first is a chemical one, $K_{eq}$, the solute adsorption equilibrium constant, defined as $C_s/C_m$, where $C_s$ is the concentration of solute adsorbed per unit accessible area of the stationary phase and $C_m$ the concentration of solute in the mobile phase at equilibrium. The second contribution is a physical one, namely the phase ratio $\phi$, defined as $A_s/V_m$, the accessible surface area of adsorbent

*Corresponding author. Fax: +1-302-831-4466.
*E-mail address:* lenhoff@che.udel.edu (A.M. Lenhoff)

0021-9673/00/$ – see front matter 
PII: S0021-9673(00)00420-9

per unit volume of mobile phase. This relationship recognizes the physicochemical nature of chromatographic retention: behavior is determined by solute partitioning between phases, governed by molecular interactions, and the phase ratio, which is a physical characteristic of the stationary phase particles.

For the chromatography of macromolecules such as proteins, the three-dimensional size and structure of the solutes relative to those of the adsorbent pore dimensions complicate the concept of defining phase ratios. Since unrestricted intraparticle diffusion requires pore radii to be much greater than the hydrodynamic radii of the chromatographic solutes [1], some fraction of the adsorbent pore volume will not be accessible to protein solutes. As a practical consequence, wider-pore adsorbents with lower surface areas can provide higher capacities for large protein solutes than the narrower pore but higher surface area adsorbents used for small molecules [2].

A more complete characterization of adsorbent pore structure, to provide information useful to practicing chromatographers, would cover the full pore size distribution (PSD), from which such quantities as the mean pore radius, the pore surface area, and phase ratio as a function of solute size can be calculated. This information would allow the effect of adsorbent physical properties to be dissected from the chemical equilibrium described in Eq. (2).

Despite the obvious utility of this level of adsorbent characterization, information of this type (with the exception of the mean pore diameter) is not routinely given by adsorbent suppliers, and therefore must be generated by the end-user. Traditional surface area measurement techniques, such as mercury porosimetry or BET nitrogen adsorption, are considered unsuitable for many of the adsorbents used for protein chromatography. Among the disadvantages given for these procedures are that: they require dry samples [3], which may result in flattening of attached hydrophilic stationary phases [4]; the small size of the solutes used inherently overestimates the surface area accessible to protein solutes [4]; and these techniques may deform or damage the adsorbent sample [5].

Inverse size-exclusion chromatography (ISEC) provides an alternative to mercury porosimetry or nitrogen adsorption for the determination of the pore size dimensions and the surface area of chromatographic stationary phases. This technique was developed by Halász [6], and has subsequently been extended and refined [7–9]. ISEC methodology has been applied to the characterization of a variety of chromatographic stationary phases, including silica [7,8,10,11], silica modified with bonded-phases [4,5,12] or coated with formamide [13], alumina [11], and a series of carbohydrate-based size exclusion gels [9]. In comparative studies between porosimetric techniques and ISEC, the ISEC method was perceived to require fewer assumptions than mercury porosimetry (e.g., contact angle and surface tension) [8], and to be superior to nitrogen adsorption for following the changes in the surface area, pore volume and pore dimensions that resulted from the grafting of polymeric coatings onto silica [10].

ISEC is applied here to characterize the physical properties of several commercially available cation-exchange adsorbents that are used for protein purification. The results described demonstrate both the practical utility of the technique for this class of adsorbents, and the ability of the technique to discern previously unknown anomalies in this adsorbent set. In a subsequent paper, we show how strongly the full PSD, rather than just the mean pore size, can influence retention on these stationary phases.

## 2. Inverse size-exclusion chromatography theory and methods

ISEC utilizes a set of standard probe molecules, of defined molecular mass and size, to examine the intraparticle pore volume of a porous material in a packed column. This examination is analogous to a molecular mass calibration in SEC; the retention volume for each standard is experimentally determined and characterized in terms of the well-known SEC distribution coefficient:

$$K_d = \frac{V_R - V_0}{V_T - V_0} \tag{3}$$

where $V_R$ is the solute elution volume, $V_0$ is the interparticle void volume and $V_T$ is the total mobile phase volume. $K_d$ values range between 0 for a totally excluded compound and 1 for compounds able to permeate and access the total pore volume. Since $(V_T - V_0)$ represents the intraparticle mobile phase volume, $K_d$ represents the extent of permeation

into the pore volume of the stationary phase material, and is independent of the column volume, the particle size of the adsorbent, and the pore volume, and is therefore suitable for comparative characterization.

The $K_d$ values for the standards are typically plotted against the log of the molecular mass, or molecular size, to prepare the SEC calibration curve. Dextrans are used here as calibration standards; these polysaccharides are readily available and are in common use for SEC calibration. The polar character of these molecules should not engender hydrophobic interactions, and ideal SEC behavior with dextrans has been achieved on anionic stationary phases [14].

The molecular size of the dextrans is given by the viscosity radius, $R_\eta$:

$$R = \left(\frac{3[\eta]M}{10\pi N_A}\right)^{1/3} \tag{4}$$

where $[\eta]$ is the intrinsic viscosity in $cm^3/g$, $M$ is the molecular mass and $N_A$ is Avagadro's number. The viscosity radius has been proposed as a universal calibration parameter for SEC as it captures the dependence of SEC elution volume on both the molecular mass and the molecular shape, as reflected in the intrinsic viscosity [15]. This size description has proven useful in SEC as it permits comparison and calibration between macromolecules of very different shapes (e.g., proteins, polysaccharides, nucleic acids and viral particles) and is independent of pore geometry and mobile phase flow-rate [15,16].

In the ISEC procedure, a pore-size distribution (PSD) is estimated from this calibration curve. Extraction of pore structural information from SEC data and subsequent calculation of other stationary phase structural parameters are based on assuming that the pore volume comprises a distribution of pores of uniform shape but different cross-sectional dimensions. These dimensions are described by a pore-size distribution function f($r$), where f($r$)d$r$ for any such function represents the pore volume that has a cross-sectional dimension in the range between $r$ and $r + dr$. The functional form that has been used most frequently (e.g., [9]) is the Gaussian relation:

$$f(r) = \exp\left[-\frac{1}{2}\left(\frac{r - r_p}{s_p}\right)^2\right] \tag{5}$$

where $r_p$ and $s_p$ are the mean and the standard deviation of the distribution respectively. The Gaussian distribution, while mathematically convenient, is physically unrealistic in permitting negative values of $r$, so that abrupt truncation of the lower end of the distribution is necessary. Alternative functions have been used as well [17]; a more realistic, yet continuous, one is the log normal distribution [18]:

$$f(r) = \frac{1}{r}\exp\left[-\frac{1}{2}\left(\frac{\log(r/r_p)}{s_p}\right)^2\right] \tag{6}$$

which is zero for $r \leq 0$. The parameters $r_p$ and $s_p$ have a less obvious physical interpretation here, but again they provide a measure of the core of the distribution and its width respectively. We have used the log normal distribution in what follows, but corresponding calculations using the Gaussian distribution yield similar results.

Calculation of $K_d$ for a given distribution is model-dependent, as a physical picture of a probe molecule partitioning in a pore is required. The standard description is of a spherical probe in a cylindrical pore, but other shapes have also been examined [7]; the analysis of Hagel et al. [9] showed very little difference for slit-like or spherical pore regions. The pores in real chromatographic stationary phases are much more irregular than any of these assumed shapes implies, and the assumption of a uniform pore shape, required for both ISEC and porosimetric techniques, can not truly represent the heterogeneous collection of geometries that comprise the pore space. Thus the pore dimensions obtained by ISEC cannot be considered absolute [9], but rather to provide functional information about stationary phases that is most relevant for comparative purposes.

Within the framework of the pore model, the distribution parameters can be related to the experimental SEC measurements. Because of the finite radius $r_m$ of the probe molecule, the part of the pore immediately adjacent to the wall is inaccessible to the center of the probe, so the fractional accessible volume is $[1 - (r_m/r)]^2$. Thus for a given probe size:

$$K_d = \frac{\int_{r_m}^{\infty} f(r)[1 - (r_m/r)^2]dr}{\int_0^{\infty} f(r)dr} \tag{7}$$

where the denominator serves for normalization. This relation shows $K_d$ to be calculated as the ratio of the pore volume accessible to a probe of radius $r_m$ to the total pore volume, consistent with the experimental definition.

The distribution parameters, in the present case $r_p$ and $s_p$, are estimated from SEC data by least-squares fitting of experimental $K_d$ values for probes covering a range of sizes. The fits in this work were performed using the IMSL (International Mathematical and Statistical Libraries) routine DRNLIN, with the integrals evaluated using the routines DQDAG and DQDAGI. An example of the agreement between fitted values and experimental $K_d$ values is shown in Fig. 1. Once f($r$) has been determined, additional distribution parameters can be calculated. The mean pore radius is found from the first moment:

$$\bar{r} = \frac{\int_0^\infty r\,\mathrm{f}(r)\mathrm{d}r}{\int_0^\infty \mathrm{f}(r)\mathrm{d}r} \tag{8}$$

The pore wall surface area required for investigating adsorption behavior, e.g., in terms of an area-based phase ratio, is found for a cylindrical pore of radius $r$ from the surface area $2/r$ available per unit pore volume. Thus the total surface area per unit pore volume is:

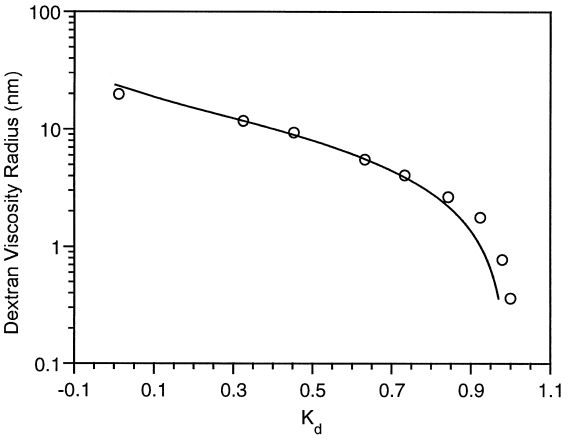


Fig. 1. Comparison of measured $K_d$ values (symbols) to the calculated calibration curve (line) for Pharmacia CM Sepharose Fast Flow.

$$A_{tot} = \frac{\int_0^\infty \frac{2}{r}\mathrm{f}(r)\mathrm{d}r}{\int_0^\infty \mathrm{f}(r)\mathrm{d}r} \tag{9}$$

However, for macromolecules it is again the accessible pore area that matters, and this is found from:

$$A(r_m) = \frac{\int_{r_m}^\infty \frac{2(r-r_m)}{r^2}\mathrm{f}(r)\mathrm{d}r}{\int_0^\infty \mathrm{f}(r)\mathrm{d}r} \tag{10}$$

These areas can be converted to other quantities such as phase ratios, again by using SEC data. For instance, since $A(r_m)$ is expressed per unit total pore volume, the phase ratio (area per unit mobile phase volume) is found by multiplication by (total included volume)/(void volume).

## 3. Materials and methods

### 3.1. Chromatographic stationary phases

Nine strong (SCX) and weak (WCX) cation-exchangers, two size-exclusion chromatographic (SEC) media and a porous silica were used for this study. The physical properties of these materials, as given by the manufacturers, are shown in Table 1.

All TosoHaas stationary phases were purchased from TosoHaas (Montgomeryville, PA, USA). Strong and weak ‘tentacle’ type cation-exchange adsorbents were purchased from EM Industries (US associate of E. Merck, Darmstadt, Germany). Silica and Spherodex cation-exchange adsorbents were purchased from BioSepra (Marlborough, MA, USA). Sepharose Fast Flow adsorbents were purchased from Pharmacia Biotech (Piscataway, NJ, USA).

The set of strong and weak cation-exchange adsorbents selected for this study differ in particle morphology, the chemical nature of the base matrix, the spacer-arm chemistry, and the density of the negatively charged groups on the resin. A brief description of the chemistry and morphological

Table 1
Physical properties, as provided by the suppliers, of the stationary phases

| Stationary phase | Functionality | Base matrix | $d_p$ (μm) | Mean pore diam. (Å) | Ion-exchange capacity (μmol/ml) |
|---|---|---|---|---|---|
| TosoHaas Toyopearl | | | | | |
| 1 SP-550 C | SCX | Methacrylate | 50–150 | 300 | 120–180 |
| 2 SP-650 M | SCX | Methacrylate | 40–90 | 1000 | 120–170 |
| 3 CM-650 M | WCX | Methacrylate | 40–90 | 1000 | 80–120 |
| 4 HW 55 F | SEC | Methacrylate | 30–60 | 300 | Not applicable |
| 5 HW 65 F | SEC | Methacrylate | 30–60 | 1000 | Not applicable |
| EM Industries | | | | | |
| 6 EMD $SO_3^-$ 650 (M) | SCX | Methacrylate | 40–90 | 1000 | Not given |
| 7 EMD $COO^-$ 650 (M) | WCX | Methacrylate | 40–90 | 1000 | Not given |
| BioSepra | | | | | |
| 8 SP Spherodex M | SCX | Dextran–silica | 40–100 | 1000 | 131 |
| 9 CM Spherodex M | WCX | Dextran–silica | 40–100 | 1000 | 131 |
| 10 Silica | None | Silica | 40–100 | 1000 | Not applicable |
| Pharmacia Biotech. | | | | | |
| 11 SP Sepharose FF | SCX | Agarose | 45–165 | Not given | 180–250 |
| 12 CM Sepharose FF | WCX | Agarose | 45–165 | Not given | 90–130 |

characteristics is given below, based on information provided by the suppliers.

### *3.1.1. TosoHaas Toyopearl*

Four Toyopearl strong and weak cation-exchange adsorbents were used: SP-550 C, SP-650 C, SP-650 M, and CM-650 M. The M and C grade materials differ in particle size, whereas the 650 and 550 denote differences in mean pore diameter, as shown in Table 1. The base matrix material for all of the Toyopearl materials is a methacrylate co-polymer. The ionizable group on the strong (SP) cation-exchangers is a sulfonated propyl group, and the weak (CM) cation-exchange ligand is a carboxy-methyl group.

The Toyopearl SEC stationary phases, HW 55 F and HW 65 F, represent the base matrix materials to which the charged ligands are chemically attached to prepare the SP and CM cation exchangers. The particle size and mean pore diameters for these chromatographic stationary phases are given in Table 1.

### *3.1.2. EM Industries*

The EMD $SO_3^-$ 650 M and EMD $COO^-$ 650 M adsorbents represent the tentacle chemistry described by Müller [19]. The synthetic strategy involves a cerium catalyzed co-polymerization of acrylamide derivatives that results in a ‘tentacle’ attached to either a methacrylate or silica support. For the 650 M materials used here, this tentacle polymerization is performed on the TosoHaas Toyopearl 65 HW methacrylate support. The resulting adsorbent is depicted as being covered with tentacles that contain 15–50 ionizable groups per tentacle and that extend outward up to 100 Å from the surface [19].

The ion-exchange capacity is not given for these products, but the presence of the polyelectrolyte tentacles suggests that it should be at least an order of magnitude higher than the conventional monolayer ion exchangers such as the Toyopearl SP and CM. The particle diameters and mean pore diameters are given in Table 1.

### *3.1.3. BioSepra*

The SP and CM Spherodex adsorbents are composite particles that are manufactured by coating spherical silica particles with dextran polymers containing ionizable groups. The SP designation for the strong cation exchanger implies a sulfonated propyl molecule as the ionizable group; however, the actual charged group is a sulfate moiety at C3 of the glucose molecule [20]. For the weak cation ex-

changer, the ionizable group is a carboxy–methyl moiety, also attached to C3 of the glucose molecule.

The mean pore diameter of the silica prior to derivatization with dextran is 1000 Å, and a sample of this base silica was also obtained. The particle and mean pore diameters are given in Table 1.

#### 3.1.4. Pharmacia Biotech

SP Sepharose Fast Flow and CM Sepharose Fast Flow are cross-linked spherical agarose supports derivatized with ionizable groups. The agarose polymers form double helical structures that are linked in bundles of 10 –10 000 helices to form an agarose network [21]. Estimates of the apparent size-exclusion pore radii of gel filtration media have been made by the manufacturer using inverse SEC [9]; the value obtained for Sepharose 6 Fast Flow (the underivatized matrix material) was 29 nm.

For SP Sepharose, the ionizable group is a sulfonate on the end of a 7-atom spacer arm attached to the support: $-O-CH_2-CHOH-CH_2-O-(CH_2)_2-CH_2SO_3^-$. Therefore, as with the BioSepra SP Spherodex, the SP designation does not describe the actual chemistry.

### 3.2. Chromatography standards

Ten dextran standards were obtained from Polymer Standards Service-USA (Silver Spring, MD, USA) and two, with $M_p$ values of 3 292 000 and 6 105 000, were received as a gift from L. Hagel (Pharmacia Biotech). The peak molecular masses ($M_p$) and solution concentrations for these standards are shown in Table 2. The values of the viscosity radius, $R_\eta$, were calculated using the equation $R_\eta = 0.0271 \times M_p^{0.498}$ [22]; these are also given in Table 2. Calf-thymus DNA was obtained from Sigma (St. Louis, MO, USA).

Table 2
Peak molecular mass ($M_p$), viscosity radius ($R_\eta$), and sample concentrations of the dextran standards used for column calibrations

| $M_p$ | $R_\eta$ (nm) | Concentration (μg/ml) |
|---|---|---|
| 180 | 0.36 | 20 |
| 830 | 0.77 | 10 |
| 4400 | 1.77 | 10 |
| 9900 | 2.65 | 10 |
| 23 400 | 4.06 | 10 |
| 43 500 | 5.53 | 10 |
| 124 000 | 9.32 | 10 |
| 196 000 | 11.7 | 10 |
| 560 000 | 19.8 | 5 |
| 1 450 000 | 31.7 | 5 |
| 3 292 000 | 47.7 | 2 |
| 6 105 000 | 64.9 | 2 |

### 3.3. Instrumentation

Glass columns of 70×1.6 cm I.D. (XK 16/70) were purchased from Pharmacia Biotech (Uppsala, Sweden). The chromatography of dextran standards was performed on a Rainin Dynamax LC System equipped with refractive index and UV detectors, and a 50-μl sample loop (Rainin Instruments, Woburn, MA, USA).

### 3.4. Chromatography of dextran standards to determine $K_d$ values

Dextran solutions were prepared by dissolving dextran in 120 m*M* NaCl and 6 m*M* sodium phosphate at pH 7, at the dextran concentrations given in Table 2. Dissolution was aided by rotation on a GlasCol rotator (Thomas Scientific, Philadelphia, PA, USA) overnight at room temperature. A DNA solution (2 mg/ml) was prepared in the same fashion. All solutions were stored at 4°C until use.

For all adsorbents, a SEC molecular calibration was generated by chromatography of the dextran standards and DNA. To prepare each adsorbent, an aliquot was settled and decanted three times in 1 *M* NaCl in 10 m*M* sodium phosphate, pH 7, prior to packing. After the third decantation, the slurry volume was adjusted to produce a suspension of approximately 50%. This suspension was added to a Pharmacia XK 16/70 column equipped with a 300-ml packing reservoir, the reservoir was filled to capacity with the NaCl–phosphate buffer, and the column was then flow packed with the same buffer at a flow-rate of 4 ml/min (300 cm/h). After packing, small amounts of adsorbent were added or removed to produce a final packed bed of 50±2 cm in length.

The standard mobile phase used for all adsorbents was 120 m*M* NaCl in 6 m*M* sodium phosphate, pH 7. For the BioSepra SP Spherodex M and EM

Industries EMD $SO_3^-$ M adsorbents, the chromatography of the dextran standards was also performed with 1 *M* NaCl in 6 m*M* sodium phosphate at pH 7. The volumetric flow-rate was 1.5 ml/min. Injection volumes were 50 μl. Peak detection was by RI for dextran standards, and UV at 260 nm for DNA. Chromatography was performed at ambient temperature. $V_0$, the interparticle void volume, was determined using DNA as the excluded solute. $V_T$, the total mobile phase volume, was determined using glucose. $K_d$ values were calculated using Eq. (3). The adsorbent porosity, $\epsilon$, was calculated using:

$$\epsilon = \frac{V_T - V_0}{V_B - V_0} \quad (10)$$

where $V_B$ is the column bed volume.

## 4. Results and discussion

### *4.1. Calibration curves, surface areas and phase ratios*

The SEC calibration curves for the different stationary phases are given in Fig. 2a (Pharmacia SP and CM Sepharose Fast Flow), Fig. 2b (TosoHaas HW 65 F, SP and CM-650 M), Fig. 2c (TosoHaas HW 55 F and SP-550 C), Fig. 2d (EM Industries EMD $SO_3^-$ and $COO^-$ M), and Fig. 2e (BioSepra SP and CM Spherodex M). For each curve, the viscosity radii of the dextran standards are plotted on a log scale against the $K_d$ values.

The curves were fitted to the log normal cylindrical pore model, the best fit parameters for which are shown in Table 3. These values were used to calculate the mean pore radius, the surface area ($A_s$) and the phase ratio ($\phi$) for each stationary phase as a function of the viscosity radius for each dextran standard. The phase ratio values and adsorbent porosity are also given in Table 3.

In order to facilitate qualitative comparisons among stationary phases, graphs of the phase ratio versus viscosity radius are given for the following groupings: Pharmacia SP and CM Sepharose FF with TosoHaas HW 65 F, SP and CM-650 M in Fig. 3a, TosoHaas HW 65 F, EMD $SO_3^-$ and $COO^-$ M in Fig. 3b, BioSepra silica, SP and CM Spherodex in Fig. 3c, and TosoHaas HW 55 F and SP-550 C in Fig. 3d. Table 4 compares the pore dimensions calculated by ISEC to those given by the stationary-phase suppliers.

From these data, meaningful comparisons of adsorbent properties, which are applicable to separation development, can be made, and these are discussed in greater detail below for specific sets of adsorbents. One such comparison is the accessible surface area per unit volume of stationary phase, as a function of solute size ($\phi$ vs. $R_\eta$). For preparative applications, where adsorbent capacity becomes important, only the surface area that is accessible to the protein of interest is chromatographically useful [23]. The information given by suppliers to characterize their materials, typically ionic capacity and mean pore diameter, are not reliable surrogates for $\phi$ vs. $R_\eta$. Comparing the ionic capacities of different adsorbents and using these to infer differences in protein capacity is misleading; the ionic capacity measurement will include all charged ligands, even those present in the smallest micropores. Likewise, as a general rule, a smaller pore diameter adsorbent should provide higher surface area and protein capacity than a larger pore diameter adsorbent; however, because $\phi$ decreases as solute size increases, this relationship is reliable only for the smallest solutes. In addition, these mean pore diameter comparisons are confounded when large polymers are derivatized or polymerized within the pores as part of the adsorbent manufacturing process.

The characterization of adsorbent PSDs by ISEC, as given below, provides a more complete assessment of accessible surface area, across the entire range of potential solute sizes. For porous stationary phases, general trends, such as the progressive loss of accessible surface area as solute size increases, are completely described. For cation exchangers prepared by polymerization reactions within the adsorbent pores, ISEC data show the change in PSDs that these reactions produce, as well as the uniformity of these changes, and provide insight into the morphology of the polymeric structures that result.

### *4.2. Pharmacia SP and CM Sepharose Fast Flow*

The calibration curves for these two adsorbents were similar (Fig. 2a), with some variation seen for two of the smaller dextran standards ($R_\eta$ of 0.77 and

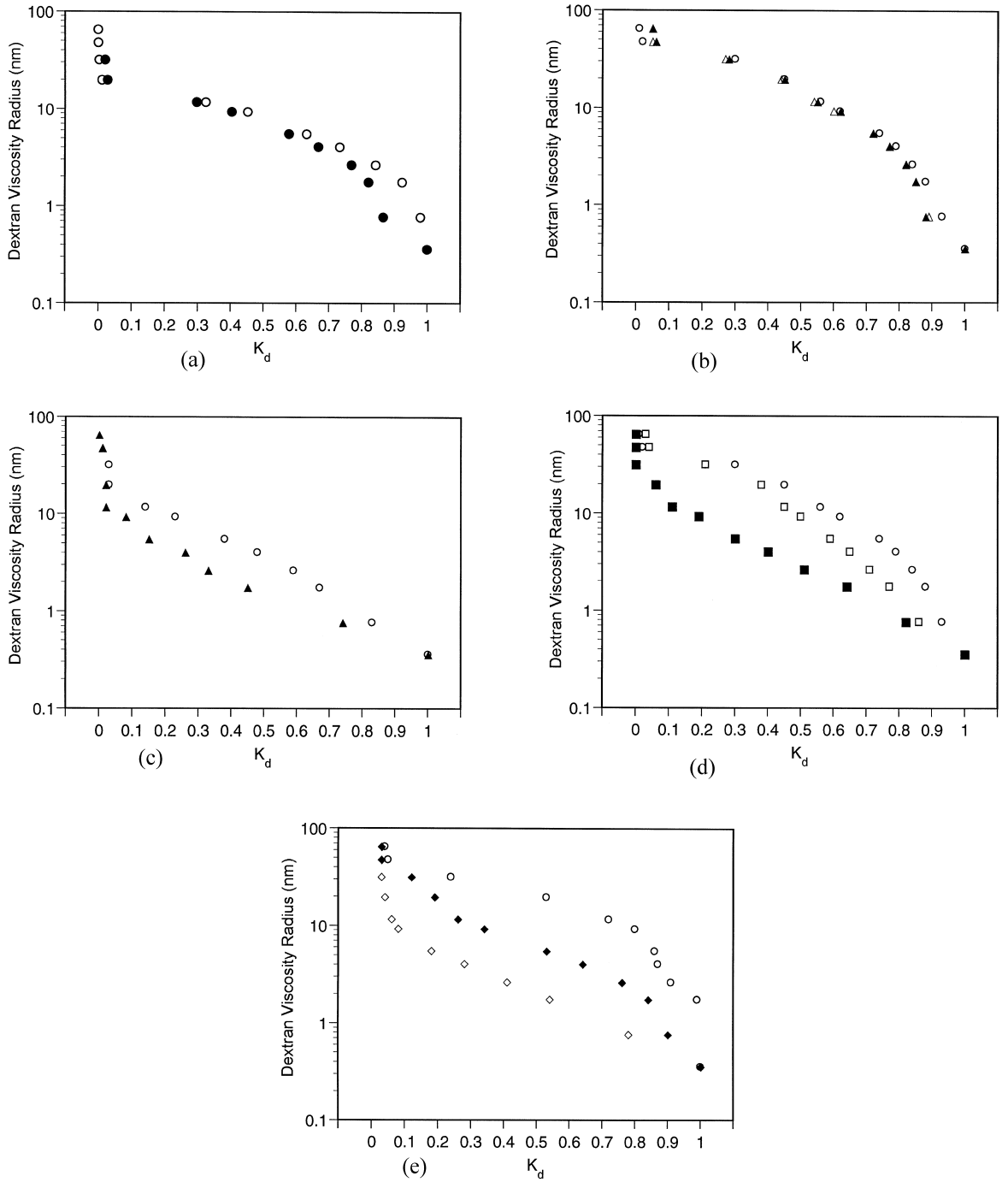


Fig. 2. (a) Dextran calibration curves for the Pharmacia SP (●) and CM Sepharose (○) fast flow cation-exchangers. (b) Dextran calibration curves for the TosoHaas HW 65 F (○) SEC stationary phase, and the TosoHaas SP (▲) and CM (△) 650 M cation-exchangers. (c) Dextran calibration curves for the TosoHaas HW 55 F (○) SEC stationary phase and the TosoHaas SP 550 C (▲) cation-exchanger. (d) Dextran calibration curves for the TosoHaas HW 65 F SEC (○) stationary phase, and the EM Industries EM $SO_3^-$ (■) and $COO^-$ (□) 650 M tentacle cation-exchangers. (e) Dextran calibration curves for the BioSepra underivatized silica (○), and the SP (♦) and CM (◇) Spherodex M cation-exchangers.

Table 3
The phase-ratio ($\phi$) as a function of dextran size for Pharmacia, TosoHaas, EM Industries, and BioSepra chromatographic stationary phases; also shown are the adsorbent porosities, and the fitting parameters, $r_p$, and $s_p$ for the log-normal pore-size distribution and the mean pore radii calculated by the ISEC method; the included volumes and void volumes, $V_T$ and $V_0$, are expressed as a fraction of the column bed volume

| Dextran standards | | $\phi$ ($m^2$/ml) | | | | | | | | | | | |
|---|---|---|---|---|---|---|---|---|---|---|---|---|---|
| $M_p$ | $R_\eta$ (nm) | SP Sepharose | CM Sepharose | TosoHaas HW 65 F | TosoHaas SP 650 M | TosoHaas CM 650 M | TosoHaas HW 55 F | TosoHaas SP 550 C $SO_3^-$ M | EMD $COO^-$ M | EMD | BioSepra 1000 Å silica | SP Spherodex M | CM Spherodex M |
| 180 | 0.36 | 50.5 | 43.8 | 23.1 | 27.1 | 28.8 | 99.4 | 181.7 | 110.7 | 64.1 | 13.8 | 75.4 | 151.9 |
| 830 | 0.77 | 46.8 | 42.8 | 22.0 | 24.6 | 26.2 | 82.6 | 132.4 | 88.2 | 51.3 | – | 71.5 | 118.6 |
| 4400 | 1.77 | 43.6 | 40.2 | 20.5 | 22.5 | 23.9 | 58.3 | 64.3 | 55.4 | 36.7 | 13.4 | 62.5 | 68.4 |
| 9900 | 2.65 | 40.6 | 37.3 | 19.3 | 20.7 | 21.9 | 43.8 | 34.9 | 37.1 | 28.8 | 12.7 | 55.2 | 41.7 |
| 23 400 | 4.06 | 35.4 | 33.0 | 17.6 | 18.0 | 19.0 | 27.9 | 16.9 | 21.1 | 21.0 | 12.1 | 45.2 | 19.2 |
| 43 500 | 5.53 | 30.3 | 28.8 | 15.8 | 15.6 | 16.4 | 17.4 | 6.2 | 11.7 | 15.9 | 11.7 | 37.0 | 8.2 |
| 124 000 | 9.32 | 19.3 | 19.8 | 11.9 | 10.7 | 11.2 | 5.8 | 1.1 | 3.7 | 9.0 | 10.6 | 22.8 | 1.3 |
| 196 000 | 11.7 | 13.1 | 14.0 | 9.8 | 8.5 | 8.8 | 2.6 | 0.2 | 1.4 | 6.6 | 9.6 | 17.3 | 0.6 |
| 560 000 | 19.8 | 0.6 | 0.4 | 5.5 | 4.5 | 4.6 | 0.2 | 0.0 | 0.3 | 3.1 | 6.7 | 7.7 | 0.1 |
| 1 450 000 | 31.7 | 0.0 | 0.0 | 2.2 | 1.7 | 1.7 | 0.1 | 0.0 | 0.0 | 1.0 | 2.8 | 2.9 | 0.0 |
| 3 292 000 | 47.7 | 0.0 | 0.0 | 0.1 | 0.2 | 0.2 | 0 | 0.0 | 0 | 0.1 | 0.3 | 0 | 0.0 |
| 6 108 000 | 64.9 | 0.0 | 0.0 | 0.0 | 0.1 | 0.1 | 0 | 0.0 | 0 | 0.1 | 0.1 | 0 | 0.0 |
| Porosity | | 0.84 | 0.84 | 0.68 | 0.63 | 0.68 | 0.70 | 0.63 | 0.69 | 0.74 | 0.67 | 0.59 | 0.65 |
| $V_T$ | | 0.90 | 0.90 | 0.81 | 0.78 | 0.81 | 0.82 | 0.78 | 0.82 | 0.85 | 0.78 | 0.74 | 0.78 |
| $V_0$ | | 0.35 | 0.35 | 0.41 | 0.41 | 0.41 | 0.38 | 0.42 | 0.42 | 0.41 | 0.41 | 0.35 | 0.37 |
| $r_p$ (nm) | | 24.2 | 27.3 | 52.7 | 51.2 | 49.7 | 13.9 | 6.8 | 11.4 | 33.3 | 68.1 | 24.1 | 8.1 |
| $s_p$ (nm) | | 0.82 | 0.99 | 0.51 | 0.41 | 0.41 | 0.44 | 2.08 | 0.42 | 0.27 | 1.06 | 0.43 | 0.49 |
| ISEC mean pore radius (nm) | | 24.7 | 27.3 | 66.1 | 76.6 | 73.9 | 19.6 | 8.8 | 16.5 | 80.5 | 68.2 | 34.3 | 10.4 |

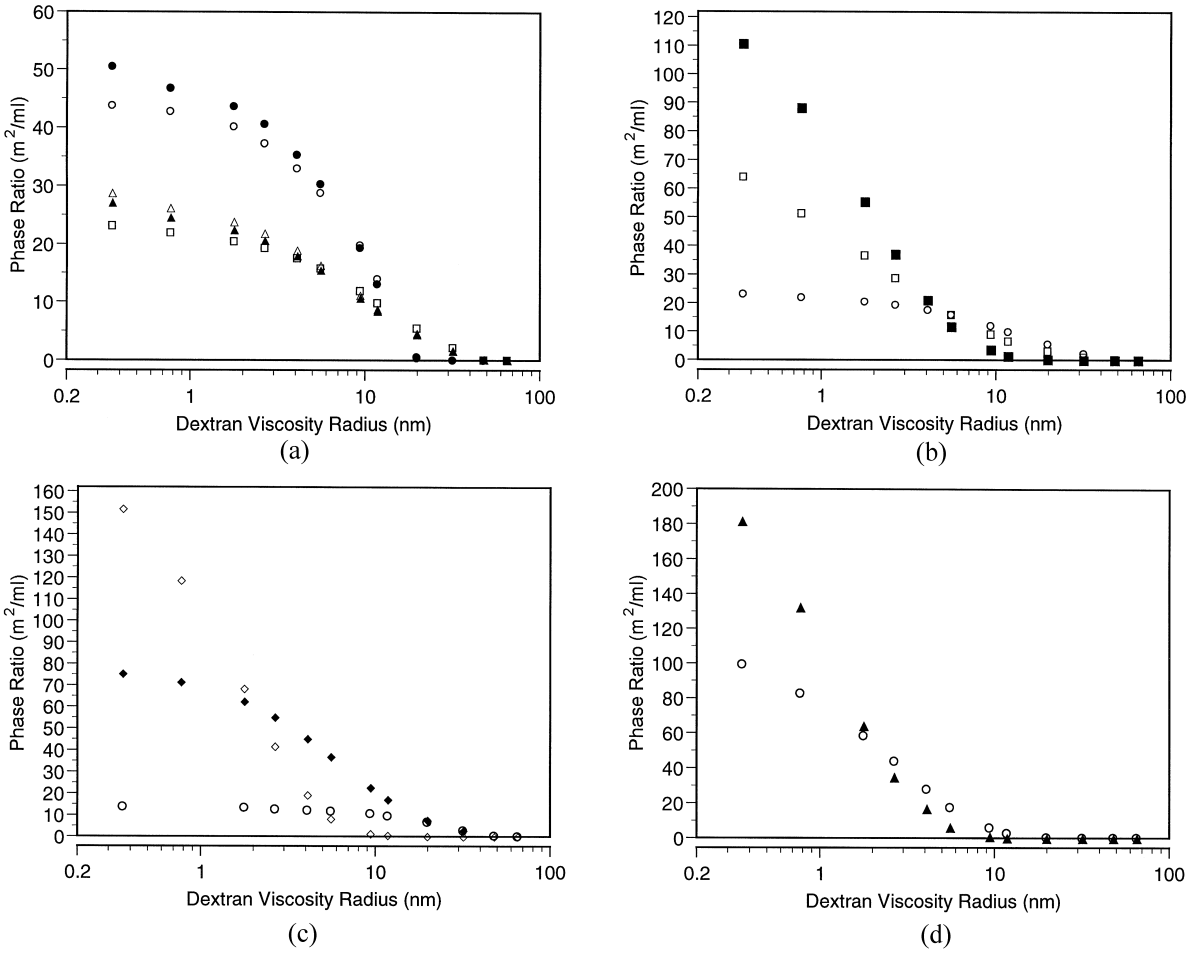


Fig. 3. (a) Phase ratios as a function of the dextran viscosity radius, $R_\eta$, for the Pharmacia SP (●) and CM (○) Sepharose Fast Flow, and the TosoHaas HW 65 F (□), and SP (▲) and CM (△) 650 M. (b) Phase ratios as a function of the dextran viscosity radius, $R_\eta$, for the TosoHaas HW 65 F (○) SEC stationary phase, and the EM Industries EM $SO_3^-$ (■) and $COO^-$ (□) 650 M tentacle cation-exchangers. (c) Phase ratios as a function of the dextran viscosity radius, $R_\eta$, for the BioSepra underivatized silica (○), and the SP (♦) and CM (◊) Spherodex M cation-exchangers. (d) Phase ratios as a function of the dextran viscosity radius, $R_\eta$, for the TosoHaas HW 55 F (○) SEC stationary phase, and the SP 550 C (▲) cation-exchanger.

1.77 nm). The longer seven-atom spacer arm of the SP Sepharose may occlude some of the smaller pore space, accounting for the loss in pore volume observed for the two smaller dextrans. The linear portion of both calibration curves spans the dextran standard size range of $R_\eta = 1.77–19.75$ nm. An ISEC mean pore radius of 24.7 nm was calculated for SP Sepharose, and 27.3 nm for CM Sepharose. Both values agree reasonably well with the radius value of 29 nm obtained by Hagel et al. [9] for Sepharose 6 Fast Flow (the underivatized base material). The difference in the fitting parameter, $s_p$, between the SP and CM adsorbents was significant, resulting in a very different PSD for the CM version, despite the similarity of the calibration curves. The occasional generation of a physically unrealistic PSD may be expected in methods such as ISEC or mercury porosimetry, which place constraints upon the pore geometry and the shape of the distribution, while adjusting the distribution itself. In these in-

Table 4
Comparison of mean pore diameters given by adsorbent suppliers and as determined by ISEC

| Stationary phase | Mean pore diameter (nm) | |
|---|---|---|
| | ISEC-calculated | As given by supplier |
| Pharmacia | | |
| SP Sepharose FF | 49.4 | – |
| CM Sepharose FF | 54.6 | – |
| TosoHaas | | |
| HW 65 F | 132.2 | 100 |
| SP 650 M | 153.2 | 100 |
| CM 650 M | 147.8 | 100 |
| HW 55 F | 39.2 | 30 |
| SP 550 C | 17.6 | 30 |
| EM Industries | | |
| EMD $SO_3^-$ M | 33.0 | 100 |
| EMD $SO_3^-$ M (1 *M* NaCl) | 59.3 | 100 |
| EMD $COO^-$ M | 161.0 | 100 |
| BioSepra | | |
| Silica | 136.0 | 100 |
| SP Spherodex M | 68.6 | 100 |
| SP Spherodex M (1 *M* NaCl) | 43.2 | 100 |
| CM Spherodex M | 20.8 | 100 |

stances, changing the pore geometry or the allowed shape of the distribution may improve the resulting fitting.

### 4.3. TosoHaas SP and CM-650 M

The calibration curves for these two cation-exchange adsorbents and the uncharged SEC material were also similar (Fig. 2b), the only differences being some variation seen for two of the smaller dextran standards ($R_\eta$ 0.77 and 1.77 nm). The linear portion of these three calibration curves spans the dextran standard size range of $R_\eta = 4.06–31.72$ nm. An ISEC mean pore radius of 66 nm was calculated for the HW 65 F, 77 nm for the SP-650 M, and 74 nm for the CM-650 M. The similar performance and pore structure of these stationary phases is consistent with the method of preparation: the base SEC material is directly derivatized with functional groups with a 1- or 3-atom spacer arm. The attachment of these short ligands onto a wide-pore material does not significantly alter the pore dimensions of the base material, and only pores of very small diameter could be significantly restricted by the introduction of these short ligands.

The larger calculated mean pore radius for the M grade cation-exchangers may point to real differences in PSDs between the M and F grade materials; however, it is also possible that differences of this magnitude ($\leq$15%) reflect difficulties in ISEC modelling of such large pore materials. In Fig. 4, the calculated PSDs are plotted for the TosoHaas HW 65 F SEC material, and the SP-650 M and CM-650 M

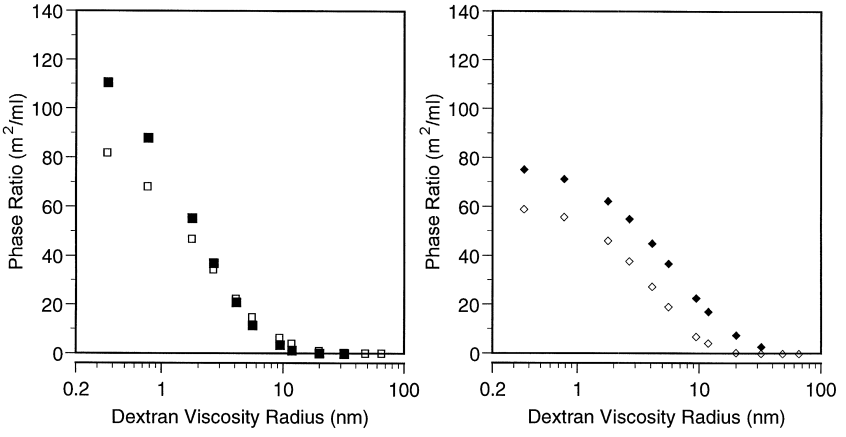


Fig. 4. (a) Phase ratios as a function of the dextran viscosity radius, $R_\eta$, for EMD $SO_3^-$ 650 M at low (0.12 M, ■) and high (1.0 *M*, □) NaCl concentrations. (b) Phase ratios as a function of the dextran viscosity radius, $R_\eta$, for SP Spherodex M at low (0.12 *M*, ♦) and high (1.0 *M*, ◊) NaCl concentrations.

cation-exchangers. All of these stationary phases contain at least some pore volume accessible to the largest dextran standards used ($R_\eta$ values of 47.72 and 64.90 nm), resulting in $K_d$ values slightly above zero. The resulting ISEC modelling fits produce PSDs that tail off gradually. The PSDs in Fig. 4 illustrate a potential source of inaccuracy that may be inherent in the fitting of dextran calibration curves to such large pore stationary phases: the more pronounced tailing of the two cation-exchangers results in larger calculated mean pore radii. This skewing from a small population of very large pores is difficult to avoid when the tested materials contain pores accessible to even the largest dextran standards. For these types of adsorbents, differences between calculated mean pore radii of $\leq$15% may not be significant.

In Fig. 3a, the phase ratio is plotted as a function of $R_\eta$ for the Pharmacia Sepharoses and the TosoHaas HW 65 F, SP and CM-650 M stationary phases. The smaller pore Sepharoses have significantly greater surface area than the TosoHaas materials for the smaller dextran solutes, but the accessible internal pore surface area decreases rapidly as $R_\eta$ increases above ~3 nm. For the Sepharoses, much of the accessible surface area is contributed by pore volume characterized by dimensions comparable to that of small proteins. For the wide pore TosoHaas materials, the loss of accessible internal pore surface area as $R_\eta$ increases is more gradual. These materials have pore space accessible to the largest dextrans ($R_\eta$ values of 47.7 and 64.9 nm), although it is limited (Table 3).

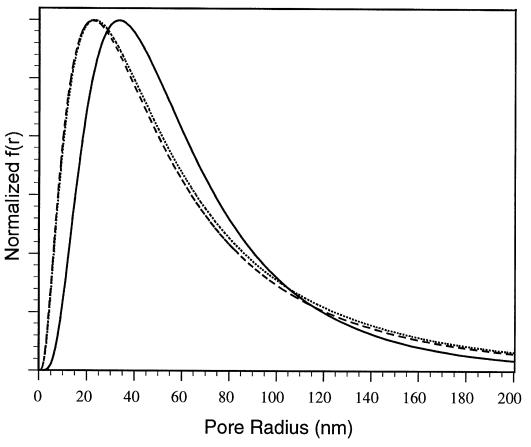


Fig. 5. Pore size distributions for TosoHaas HW 65 F (———) SEC stationary phase, and the SP (· · ·) and CM (- - -) 650 M cation-exchangers.

### *4.4. EM Industries EMD $SO_3^-$ M and EMD $COO^-$ M*

The EM Industries cation-exchangers are prepared by the polymerization of polyelectrolyte chains onto a TosoHaas HW 65 base material. These polyelectrolytes are envisioned to form 'tentacles' extending some 10 nm outward from the adsorbent surface [19]. Several groups have previously reported on the protein capacity and the kinetics of adsorption of these 'tentacle-type' adsorbents [24–27]; however, the effect of the polymerization on pore volume and pore-size distribution has not been examined.

The dextran calibration curves for the base HW 65 F SEC material and the EMD $SO_3^-$ M and $COO^-$ M tentacle adsorbents are shown in Fig. 2d. The shift of the calibration curves for the EMD $SO_3^-$ M and $COO^-$ M to the left, relative to the base HW 65 F SEC material, indicates that the polymerization of the polyelectrolyte tentacles has significantly decreased the pore dimensions of the SEC base material. This reduction in pore dimensions appears significantly greater for the EMD $SO_3^-$ M than the EMD $COO^-$ M.

The pore dimensions determined by ISEC are given in Table 3. The mean pore radius of 16.5 nm calculated for the EMD $SO_3^-$ M is much smaller than the value of 66.1 nm obtained for the base HW 65 F material, but the calculated mean pore radius of the EMD $COO^-$ M is larger, at 71 nm. As observed with the TosoHaas cation-exchangers, the calculated mean pore radius of the EMD $COO^-$ M is dominated by modelling and fitting issues associated with large pore materials, and does not represent the extent of the polymerization reaction. The calculated PSDs of the TosoHaas HW 65 F and the EMD $SO_3^-$ and $COO^-$ M stationary phases are shown in Fig. 5. For the EMD $COO^-$ M adsorbent, the distribution is clearly widened relative to the base material, with significantly more pore volume accessible only to the smaller dextran solutes, but with large pores clearly retained after the polymerization. This would seem consistent with the supplier's representation of tenta-

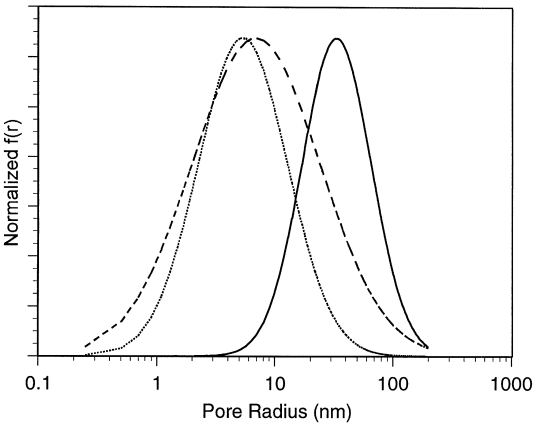


Fig. 6. Pore size distributions for TosoHaas HW 65 F (———) SEC stationary phase, and the EM Industries EMD $SO_3^-$ (· · ·) and $COO^-$ (- - -) 650 M tentacle cation-exchangers.

cles up to 10 nm in length, which would generate a minimal restriction in the largest pores ($R_\eta > 100$ nm) present in the HW 65 base material, but would become increasingly more pronounced for the smaller pores in the distribution, which would then become significantly smaller. For the EMD $SO_3^-$ M adsorbent, the calculated PSD in Fig. 5 does reveal significant loss of the large pores present in the base material.

The substantial pore size reduction for the EMD $SO_3^-$ M indicates a polymerization more extensive than previously described for the tentacle representation. In Table 3 and Fig. 3b, the effect of this internal pore polymerization on the surface area and phase ratio as a function of $R_\eta$ is shown. As compared to the HW 65 F, the surface area accessible to the small dextran solutes ($R_\eta \leq 1.77$ nm) is increased ~2 fold for the EMD $COO^-$ M, and 4–5 fold for the EMD $SO_3^-$ M. The much greater increase in surface area for the EMD $SO_3^-$ M is consistent with the 'tentacle' morphology, but the tentacles appear to be much longer than 10 nm. The effect would be analogous to creating multiple smaller regions of pore space among the polymeric tentacles within the pores of the base material. Of course, a cylindrical pore is a very poor representation of this internal structure, but the distribution of pore volume with linear dimension should still be captured reasonably well.

The area calculations are less reliable quantitatively, but should also still capture the right trend. The loss of pore volume accessible to large solutes for the EMD tentacle adsorbents can be seen in Table 3 and Fig. 3b, which show the phase ratios calculated for solutes of $R_\eta \geq 9$ nm being progressively decreased, relative to the HW 65 F base material. For solutes with $R_\eta \leq 4.06$ nm, the introduction of tentacles results in significantly increased surface area, particularly for the EMD $SO_3^-$ M adsorbent. From the viewpoint of functional preparative capacity, this polymerization would be expected to increase the capacity of these adsorbents for small or average size proteins, but to decrease the capacity for large macromolecules, as compared to the TosoHaas SP and CM-650 M materials.

### *4.5. BioSepra silica, SP and CM Spherodex*

The BioSepra Spherodex adsorbents are prepared by a covalent coupling of a sulfated or carboxymethylated dextran to a porous silica matrix. The effects of this process on pore dimensions, surface areas, and phase ratios are shown in Table 3 and Fig. 3c. As observed for the EMD tentacle materials, the addition of the ionizable dextran coating results in a significant decrease in pore dimensions, and the formation of a permeable gel network within the silica pores. The extents of the pore occlusion for the SP Spherodex and the CM Spherodex are significantly different. The ISEC mean pore radius was calculated to be 68.3 nm for the base matrix silica, 34 nm for the SP Spherodex M, and 10 nm for the CM Spherodex M. The more extensive intraparticle gel formation for the CM Spherodex results in a much higher surface area for small solutes ($R_\eta \leq 1$ nm) measured for the CM Spherodex relative to both the SP Spherodex and the base silica matrix. Surface area decreases with increasing $R_\eta$ more rapidly for the CM Spherodex (Fig. 3c); this indicates that a denser intraparticle polymer network is formed with smaller spaces through which the dextrans can diffuse. However, these spaces would be largely inaccessible to large proteins. The CM Spherodex would provide high capacity for small proteins, with little accessible surface area for large proteins; the SP Spherodex would have good capacity over a broader range of protein sizes, but at the expense of the very high capacity at the small end of the size range seen for the CM version.

### 4.6. TosoHaas HW 55 F and SP-550 C

These TosoHaas stationary phases are smaller pore diameter versions of the HW 65 F and SP-650 M materials respectively. Unlike their large pore counterparts, there are significant differences in the pore dimensions, surface area, and phase ratios between the base material and the derivatized SP-550 C. Table 3 and Fig. 3d show the surface areas and phase ratios as a function of solute size for these materials. As with the BioSepra and EM adsorbents, the derivatized SP-550 C showed a significant increase in surface area for the smaller dextran standards, decreased accessibility to the internal pore surface area for larger solutes, and a decrease in pore dimensions relative to the underivatized HW 55 F. A mean size-exclusion radius of 20 nm was calculated for the HW 55 F, as compared to only 9 nm for the SP-550 C (Table 3). This difference in pore size was not seen for the 65 F and SP and CM-650 M, which are substantially equivalent in pore dimensions and surface area. The reason for the large differences between the pore characteristics of the HW 55 F and SP-650 C is not clear. One possible explanation would be that the F grade SEC stationary-phase has either a different PSD or a different method of manufacture to that of the C grade used to prepare the SP-550 C adsorbent.

The derivatization of the base HW 55 material with a propane sulfonic acid moeity would not be expected to alter the pore dimensions to the extent measured by ISEC. The calibration curves for the HW 55 F and the SP-550 C are significantly different, as seen in Fig. 2c. The functional result of this pore size decrease is to produce an adsorbent of which the accessible surface area decreases rapidly as solute size increases. The SP-550 C provides a high surface area for peptides and small proteins; for these solutes it could provide capacity advantages over the other adsorbents tested. This advantage exists over a relatively narrow range of solute sizes; as an example, comparison to the TosoHaas SP-650

Table 5
The phase-ratio ($\phi$) as a function of dextran size for the BioSepra SP Spherodex and the EMD $SO_3^-$ M cation-exchangers, determined at 0.12 and 1 *M* NaCl. Also shown are the adsorbent porosities, the fitting parameters, $r_p$ and $s_p$, for the log-normal pore-size distribution, and the mean pore radii calculated by the ISEC method. The included volumes and void volumes, $V_T$ and $V_0$, are expressed as a fraction of the column bed volume.

| Dextran standards | | $\phi$ | | | |
|---|---|---|---|---|---|
| $M_p$ | $R_\eta$ | SP Spherodex M | | EMD $SO_3^-$ M | |
| | (nm) | (0.12 *M* NaCl) | (1 *M* NaCl) | (0.12 *M* NaCl) | (1 *M* NaCl) |
| 180 | 0.36 | 75.4 | 59.0 | 110.7 | 81.9 |
| 830 | 0.77 | 71.5 | 55.9 | 88.2 | 68.1 |
| 4400 | 1.77 | 62.5 | 46.3 | 55.4 | 46.8 |
| 9900 | 2.65 | 55.2 | 37.9 | 37.1 | 34.4 |
| 23400 | 4.06 | 45.2 | 27.5 | 21.1 | 22.2 |
| 43500 | 5.53 | 37.0 | 19.2 | 11.7 | 14.8 |
| 124 000 | 9.32 | 22.8 | 7.0 | 3.7 | 6.4 |
| 196 000 | 11.7 | 17.3 | 4.3 | 1.4 | 4.0 |
| 560 000 | 19.8 | 7.7 | 0.4 | 0.3 | 1.0 |
| 1 450 000 | 31.7 | 2.9 | 0.1 | 0.0 | 0.1 |
| 3 292 000 | 47.7 | 0.0 | 0.0 | 0.0 | 0.0 |
| 6 108 000 | 64.9 | 0.0 | 0.0 | 0.0 | 0.0 |
| Porosity | | 0.59 | 0.53 | 0.69 | 0.62 |
| $V_T$ | | 0.74 | 0.71 | 0.82 | 0.77 |
| $V_0$ | | 0.35 | 0.37 | 0.42 | 0.40 |
| $r_p$ (nm) | | 24.1 | 18.3 | 11.4 | 17.8 |
| $s_p$ (nm) | | 0.43 | 0.56 | 0.42 | 0.36 |
| ISEC mean pore radius (nm) | | 34.3 | 21.6 | 16.5 | 29.6 |

M (Table 3) shows that for solutes of $R_\eta > 2.65$ nm, capacities should be equivalent to or greater than those for the larger pore SP-650 M.

### *4.7. Effect of NaCl concentration on phase ratios and pore dimensions*

For the SP Spherodex M and the EMD $SO_3^-$ M, the dextran chromatography was also carried out in 1 M NaCl to characterize further the morphology of the intrapore polymers present in these adsorbents. The three-dimensional arrangement of these polymers within the pore space is influenced by electrostatic repulsion within and between polyelectrolyte chains. Screening of these charges by increasing ionic strength permits detection of changes in the three-dimensional structure that affect the pore dimensions. A comparison of pore dimensions and phase ratios determined under different NaCl concentrations is given in Table 5 and Fig. 6.

The effect of increasing the NaCl concentration on pore dimensions was very different for the two adsorbents tested. For the EMD $SO_3^-$ M, the calculated mean pore radius increased from 17 nm at 0.12 *M* NaCl to 30 nm at 1 *M* NaCl. The $\phi$ vs. $R_\eta$ plots at 0.12 and 1 *M* NaCl (Fig. 6) show divergence between the calculated phase ratios for smaller solutes. The large increase in the calculated mean pore radius at high salt concentration indicates a mobile polymeric phase, one that is able to undergo a significant collapse and compaction. This would be consistent with the behavior of very long linear tentacles, with little or no cross-linking to lock the polymeric structure in place. In the collapsed state, this polymer phase is still permeable to the smallest dextran standards ($R_\eta \leq 1.77$ nm) but less so than in the extended state, resulting in the divergence seen in Fig. 6 for the smaller solutes.

For SP Spherodex M, the calculated mean pore radius decreased from 34 nm at 0.12 *M* NaCl to 22 nm at 1 *M* NaCl. In the $\phi$ vs. $R_\eta$ plots at 0.12 *M* and 1 *M* NaCl (Fig. 6), the offset between the two curves is nearly uniform across the entire dextran size range. At low ionic strength, charge repulsion between the polyelectrolytes apparently provides some three-dimensional structuring of the polymer phase; some of the open areas and diffusion pathways within the polymer are the result of repulsive effects that prevent proximate location of the polymer chains. The charge shielding at high ionic strength allows the polyelectrolytes to achieve closer proximity, reducing the permeability of this intrapore polymer phase to dextran standards. Unlike the tentacle morphology, which allows significant compaction, the sulfated dextran polymers within the Spherodex pores appear to be anchored at both ends spanning the pore, with significant cross-linking, forming a gel within the pore space. This gel has limited ability to contract toward the pore walls, but the relative positioning of the polymers within the gel can change, making it more (low salt) or less (high salt) permeable.

## 5. Conclusions

ISEC has been used to characterize several commercial cation-exchange adsorbents. As shown in Table 4, the calculated mean pore dimensions were in reasonably good agreement with the suppliers' information for adsorbents prepared via a traditional coverage of CM or SP ligands. Adsorbent preparation strategies in which ionizable groups were introduced via polymerization (EM Industries) or grafting of dextran polymers (BioSepra) were found to have significant effects on the pore dimension and surface area of the base materials. For these stationary phases, the pore dimensions provided by the suppliers did not reflect these modifications, and therefore were not in agreement with the dimensions determined by ISEC.

The extent of the alteration of pore dimensions was found to be significantly different for the CM and SP versions for both the BioSepra and EM Industries stationary phases. Some degree of variability may be inherent in the preparation of these adsorbents. ISEC provides the end-user with a convenient method for discerning these manufacturing anomalies.

ISEC calculations also provide a characterization of the accessible internal pore surface area, as a function of solute size. As macromolecular solute size increases, accessible surface area decreases significantly, complicating the selection of high capacity preparative adsorbents for the purification of large or multimeric proteins, vaccine antigens or

viruses. Because ISEC utilizes a solute series that ranges over two orders of magnitude in $R_\eta$, the entirety of adsorbent permeability is assessed. The resulting characterization permits the selection of adsorbents with pore dimensions and surface area suitable for the solute size for which it is intended.

## Acknowledgements

We are grateful for support from the National Science Foundation (grant number CTS-9321318). The authors thank Lars Hagel for providing dextran standards, and for helpful discussions about inverse size-exclusion chromatography methods.

## References

[1] W.M. Deen, AIChE J. 33 (1987) 1409.
[2] W. Kopaciewicz, S. Fulton, S.Y. Lee, J. Chromatogr. 409 (1987) 111.
[3] S. Kuga, J. Chromatogr. 206 (1981) 449.
[4] I. Mazsaroff, F.E. Regnier, J. Chromatogr. 442 (1988) 15.
[5] H. Guan, G. Guiochon, J. Chromatogr. A 731 (1996) 27.
[6] I. Halász, K. Martin, Angew. Chem. Inter. Ed. (Engl.). 17 (1978) 901.
[7] J.H. Knox, H.P. Scott, J. Chromatogr. 316 (1984) 311.
[8] J.H. Knox, H.J. Ritchie, J. Chromatogr. 387 (1987) 65.
[9] L. Hagel, M. Östberg, T. Andersson, J. Chromatogr. 743 (1996) 33.
[10] K. Jerabek, A. Revillon, E. Puccilli, Chromatographia 36 (1993) 259.
[11] L.Z. Vilenchik, J.A. Asrar, R.C. Ayotte, L. Ternorutsky, C.J. Hardiman, J. Chromatogr. 648 (1993) 9.
[12] W. Werner, I. Halász, J. Chromatogr. Sci. 18 (1980) 277.
[13] R. Nikolov, W. Werner, I. Halász, J. Chromatogr. Sci. 18 (1980) 207.
[14] P.L. Dubin, M.M. Tecklenburg, Anal. Chem. 57 (1985) 275.
[15] M. Potschka, Anal. Biochem. 162 (1987) 47.
[16] M. Briššová, M. Petro, I. Lacík, A.C. Powers, T. Wang, Anal. Biochem. 2423 (1996) 104.
[17] J.E. Harlan, D. Picot, P.J. Loll, R.M. Garavito, Anal. Biochem. 224 (1995) 557.
[18] G.A. Korn, T.M. Korn, in: Mathematical Handbook For Scientists and Engineers, 2nd ed., McGraw-Hill, New York, 1968, p. 674.
[19] W. Müller, J. Chromatogr. 510 (1990) 133.
[20] BioSepra Product Bulletin Lit. Code BT205102 (1992)
[21] S. Arnott, A. Fulmer, W.E. Scott, I.C.M. Dea, R. Moorhouse, D.A. Rees, J. Mol. Biol. 90 (1974) 269.
[22] L. Hagel, in: P.L. Dubin (Ed.), Aqueous Size-exclusion Chromatography, Elsevier, Amsterdam, 1988, p. 119.
[23] C. Chang, A.M. Lenhoff, J. Chromatogr. A 827 (1998) 281.
[24] R. Janzen, K. Unger, W. Müller, M.T.W. Hearn, J. Chromatogr. 552 (1990) 77.
[25] M.T.W. Hearn, A.N. Hodder, F.W. Fang, M.I. Aguilar, J. Chromatogr. 548 (1991) 117.
[26] F. Fang, M.I. Aguilar, M.T.W. Hearn, J. Chromatogr. A 729 (1996) 49.
[27] F. Fang, M.I. Aguilar, M.T.W. Hearn, J. Chromatogr. A 729 (1996) 67.